Mechanism and Interface Study of One-to-one Metal NP/Metal Organic Framework Core-shell Structure

Author: Furui Zhang

Mechanism and Interface Study of One-to-one Metal NP/Metal Organic Framework Core-shell Structure

Furui Zhang

A thesis submitted to the Faculty of

the department of Chemistry

in partial fulfillment

of the requirements for the degree of

Master of Science

Boston College
Morrissey College of Arts and Sciences
Graduate School

07/2017

Mechanism and Interface Study of One-to-one Metal NP/Metal Organic Framework Core-shell Structure

Furui Zhang

Advisor: Prof. Chia-Kuang Tsung

Abstract

The core-shell hybrid structure is the simplest motif of two-component systems which consists of an inner core coated by an outer shell. Core-shell composite materials are attractive for their biomedical, electronic and catalytic applications in which interface between core and shell is critical for various functionalities. However, it is still challenging to study the exact role that interface plays during the formation of the core-shell structures and in the properties of the resulted materials. By studying the formation mechanism of a well interface controlled one-to-one metal nanoparticle (NP)@zeolite imidazolate framework-8 (ZIF-8) core-shell material, we found that the dissociation of capping agents on the NP surface results in direct contact between NP and ZIF-8, which is essential for the formation of core-shell structure. And the amount of capping agents on the NP surface has a significant effect to the crystallinity and stability of ZIF-8 coating shell. Guided by our understanding to the interface, one-to-one NP@UiO-66 core-shell structure has also been achieved for the first time. We believe that our research will help the development of rational design and synthesis of core-shell structures, particularly in those requiring good interface controls.

TABLE OF CONTENTS

LIST OF TABLES

LIST OF FIGURES

LIST OF ABBREVIATION

MOF	Metal Organic Framework
ZIF-8	Zeolite Imidazolate Framework-8
CTAB	Cetyltrimethylammonium Bromide
CTAC	Cetyltrime-thylammonium Chloride
PVP	Polyvinylpyrrolidone
MUA	11-Mercaptoundecanoic acid
SEM	Scanning Electron Microscope
TEM	Transmission Electron Microscope
ICP-OES	Inductively Coupled Plasma-Optical Emission Spectrometry
PXRD	Powder X-Ray Diffraction
2-mim	2-Methylimidazole
SAED	Selected Area Electron Diffraction
Pd@SC-ZIF-8	Pd@Single-Crystalline ZIF-8
Pd@PC-ZIF-8	Pd@Poly-Crystalline ZIF-8

Chapter 1: Introduction

Nanomaterials, by definition, are materials in the nanometer scale (≤100 nm). Compared with bulk materials, they obtain advantages such as increased surface area to volume ratio and high surface energy. The synthesis techniques of nanomaterials fall into three main categories: i) vapor condensation, ii) colloidal chemical reaction and iii) solid state processes. Through these synthetic techniques not only one-phase pure nanomaterial can be synthesized, but also composite or hybrid nanomaterials composed of more than one materials can be obtained. Typically, core-shell structure, denominated in a concentric hybrid semiconductor material during the early 1990s,[1,2] draws lots of attention not only because it combines two different materials together, but also because new properties brought by the new interface created. For example, in semiconductor core-shell structure, appropriate coating shell provides passivation of surface trap states resulting in enhanced fluorescence quantum yield.[3]

However, in the field of heterogeneous catalysis, interface study is rare for core-shell materials. For example, coating metal NPs with porous materials are very popular method to develop hybrid materials recently. Most of the works focus on the advantages resulted from physical barrier effect of coating shell, like sieving effect, keep entities larger than the window size away from active sites on metal NPs surface. In fact, understanding interface environment is critical to develop intermediate selective heterogeneous hybrid materials, as the selectivity comes from well-defined spatial and chemical environment around the active sites at the interface. Thus, metal organic frameworks become a very promising candidate to realize this goal, since MOFs are crystalline porous materials with

long range order whose pore environment can be fine-tuned via various post-synthetic modification methods. Making use of the tunability of MOFs to control catalytic properties of metal NPs@MOFs core-shell structure is one of the promising future directions in this field.[4,5]

This thesis focuses on the behavior of capping agents at the interface during the formation of a unique one-to-one NP@MOF core-shell structure. The interface understanding helps us develop a novel synthetic strategy of NPs@MOFs core-shell structure and also facilities the development of intermediate selective hybrid core-shell materials.

1.1 Metal NPs: Surface Environment and Catalytic Properties

Heterogeneous catalysts are considered more appropriate catalyst for industry use because of the ease of separation/recycle and the possibilities to use a fixed-bed reactor. Supported palladium/carbon catalysts are frequently used in hydrogenation and coupling reactions. [6,7] However, compared with homogeneous catalysts whose catalytic properties can be well-controlled by artificially fine tune the coordinated ligand around metal center, tuning the catalytic properties of heterogeneous catalysts is challenging (Figure 1).[8] For one reason, the active sites of heterogeneous catalysts are more complex than homogeneous ones: various coordination sites, including terrace, edge, kink, or corner sites, are present on a metal nanoparticle surface and results in different catalytic properties. For another reason, there are lots of factors that influence the coordination environment leading to different properties. Organic molecules array, like capping

agents, on metal NPs surface could change the spatial environment on the metal NPs surface. For example, the influence of an amine capping agents layer to the selectivity of Pt_3Co in cinnamaldehyde hydrogenation reaction was discussed by B. Wu and et.[9] Loading metal NPs on a support also generates different local environments because of metal-support interaction. Single site heterogeneous catalysts are considered as next generation heterogeneous catalysts in which support effect is a critical topic needs to be well studied. [10-12]

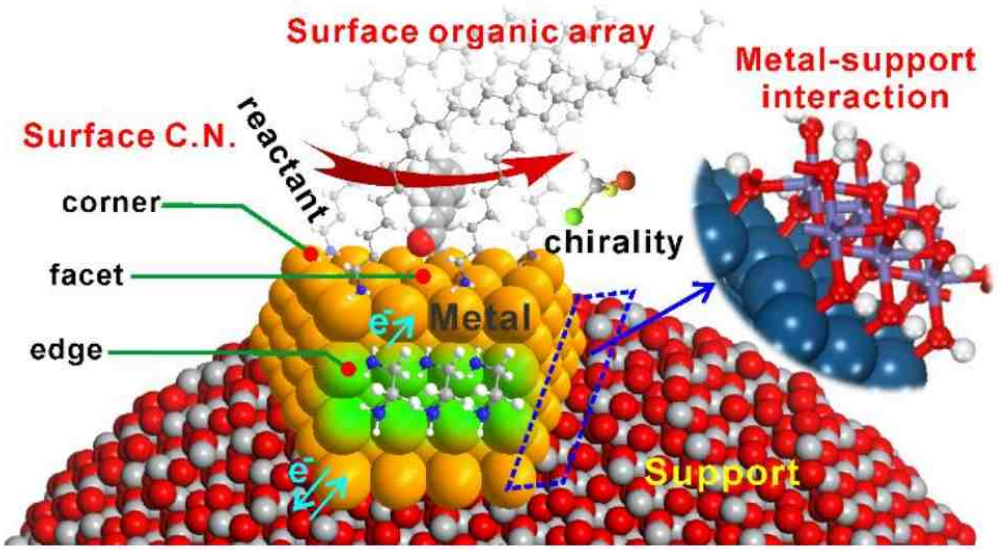

Figure 1. Involvement of factors that affect coordination environment around active sites on heterogeneous metal NPs: coordination number difference (corner, facet, or edge); surface organic molecules array affects reactant's interaction between metal NPs; electronic effect induced by surface coordinated ligands; the local environments of metal-support effect. Copyright © American Chemical Society 2017

Up to now, a systematic method to well control coordination environment around active metal atomic sites on heterogeneous catalysts is absent and highly desired. Coating metal

NPs with crystalline porous materials with molecular level tunability is a promising way to realize this. By fine tuning the environment of the porous structure, at the interface, the spatial of chemical environment around active sites are also capable of being changed. Thus, with long range order and high tailorability, metal organic frameworks, as one of the most attractive crystalline porous materials, were chosen to obtain metal NPs@porous mateirals core-shell structure.

1.2 Metal NPs@Metal Organic Frameworks Core-Shell Structure

1.2.1 Properties Resulted from MOFs as Coating Shell

NPs@MOFs core-shell structures normally can be classified as three types: one-to-one NP@MOF, multiple NPs@MOF and york-shell NP@hollow MOF (Figure 2). Difference in encapsulation forms brings about different properties and performance. One-to-one NP@MOF core-shell structure provides uniform shell thickness and diffusion length which benefits kinetic study closely related to diffusion. Metal NPs size in NPs@MOF core-shell structure are normally smaller (<10 nm) which results in higher activity, but the spatial distribution of metal NPs in MOFs is less controllable with only few studies published.[13-21] Spatial restriction of catalysts in york-shell NP@MOF structure is much less compared with other two types of core-shell structures and this is more vital when homogeneous catalysts are incorporated in MOFs.[22] In this thesis, well-controlled formation and mechanism study of these three types of NPs/MOFs composite materials are discussed based on quaternary ammonium surfactants capped metal NPs.

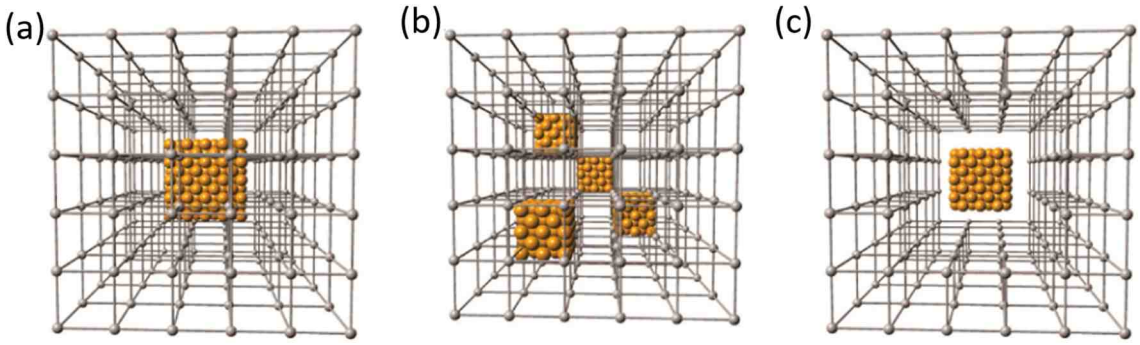

Figure 2. (a) One-to-one NP@MOF. (b) multiple NPs@MOF. (c) york-shell NP@hollow MOF. Copyright © American Chemical Society 2014.

Coating metal NPs with porous materials is a new approach to enhance the catalytic performance of metal nanoparticels. As other porous materials, MOFs around metal NPs could provide physical protective barrier preventing metal NPs from aggregating or sintering together which decreases the catalytic activity. Also, since each MOF has a unique structure with specific window/aperture size, sieving effect can be realized by coating heterogeneous catalysts with MOFs, and thus size selectivity can be imparted. Compared with other porous materials, like silica, firstly, MOFs have nanoscale pores having more obvious impact to diffusion effect. Secondly, the chemical compositions and topological structures of MOFs can be vastly varied with over 20,000 different MOFs being reported in the past decade. Thirdly, the nature of coordination interaction between metal node and organic linkers in MOFs allows reversible modification even after the synthesis.

Taking advantage of the tunability of MOFs to modulate catalytic performance in hybrid heterogeneous materials has been considered as one of the main future directions in MOFs based heterogeneous catalysis.[4] One of the main reasons is that post-synthetic

modification methods of MOFs are undergoing a fast development. Various methods have been developed to modify pore environment after MOFs synthesis based on either the metal nodes[23] or organic linkers, such as solvent assisted linker exchange,[24-28] atomic layer deposition in MOFs[29,30] and solvent assisted linker incorporation.[31,32] However, there is no report yet discussing the influence the change of pore environment brings to the catalytic performance. Since the catalytic reactions in NPs@MOFs core-shell composite materials happen around the active sites on NPs surface, which is at the interface between metal NPs and MOFs, the study of interface environment is critical before real control of catalytic properties of the hybrid material.

1.2.2 Approaches to Synthesize Metal NPs@MOFs

Generally, there are three ways to synthesize metal NPs@MOFs core-shell structures: i) introduction of MOFs into metal precursor solution in which metal precursors are reduced to form metal NPs inside of MOFs or on the external surface of MOFs; ii) introduction of as-synthesized metal NPs (always with capping agents) in to MOFs synthetic solution (mixture of metal node and organic linker) to enclose metal NPs with MOFs shell; iii) one pot synthesis with metal NPs reduced and MOFs formed simultaneously.

When MOFs crystals are introduced into metal precursor solution of metal NPs, because of capillary effect of MOFs pores, liquid containing metal NPs precursors spontaneously penetrate MOFs pores. Under the reducing environment, metal precursors are reduced and form metal NPs. In this case, the morphology and size of metal NPs are not well

controlled and affected by the intrinsic nature of pores in MOFs. Also, metal NPs are often formed on the external surface of MOFs as well. Thus, the shape, size, morphology and distribution of metal NPs cannot be well controlled by using this method.

One pot/step synthesis of NPs/MOFs materials by mixing metal precursors of metal NPs and starting materials of MOFs simultaneously. By doing so, controlled reduction of metal precursors inside MOFs pore or preferential growth of MOFs on generated metal NPs needs to be realized. Generally, this method is less controllable and the product is less predictable because of the complexity of the synthetic environment.

Synthesizing metal NPs in advance of introducing MOFs starting materials solution is also called “bottle-around-ship” method. The advantages of this method is that, because of well-studied shape-, size-controlled metal NPs synthetic methods, the properties of as-synthesized metal NPs can be fine-tuned before encapsulation and so does MOFs shell. Two critical problems need to be solved: controlled formation of MOFs around metal NPs instead of homogeneous nucleation in solution; protection of metal NPs from agglomeration under MOFs growth condition. Thus, surface modifications of metal NPs like capping agent exchange are often carried out to facilitate interaction between MOFs clusters and metal NPs surface, also to well protect metal NPs with high surface energy from aggregation. However, using strong capping agents results in an indirect contact interface with capping agents in between metal NPs and MOFs. This is undesired when catalytic properties of metal NPs cores want to be tuned by controlling pore environment of MOFs at the interface. Thus, a direct contact between metal NPs and MOFs is urgently

desired to make use of tunability of MOFs in fine-tuning catalytic performance of NPs/MOFs hybrid materials.

Chapter 2 Experimental Section

2.1 Chemical and Materials

Cetyltrimethylammonium bromide (CTAB, Calbiochem, 98%), hexadecyltrimethyl-ammonium chloride (CTAC, TCI, 95%), ascorbic acid (Sigma-Aldrich, 99%), hydrogen tetrachloroaurate trihydrate ($HAuCl_4 \bullet 3H_2O$, Sigma-Aldrich, ~50% Au basis), hygrogen tetrachloropalladate (H_2PdCl_4, Sigma-Aldrich, 98%), zinc nitrate hexahydrate ($Zn(NO_3)_2 \bullet 6H_2O$, J.T. Baker, 99%), 2-methylimidazole (Alfa Aesar, 97%), sodium bromide (NaBr, Sigma-Aldrich, 99%), sodium citrate tribasic dihydrate (trisodium citrate, Sigma-Aldrich, 99.5%), sodium boronhydride ($NaBH_4$, Sigma-Aldrich, 98%), silver nitrate ($AgNO_3$, Sigma-Aldrich, 99%), ammonium hydroxide solution ($NH_3 \bullet H_2O$, Sigma-Aldrich, 28-30%), D-(+)-glucose (Sigma-Aldrich, 99.5%), crotonaldehyde (predominantly trans, Sigma-Aldrich, 99%), deuterium oxide (Cambridge Isotope Laboratory, D-99.9%), chloroform-D (Cambridge Isotope Laboratory, D-99.8%), zirconyl chloride octahydrate ($ZrOCl_2$, Acros Organics, 98%), tetrafluoroterephthalic acid (BDC-4F, Sigma-Aldrich, 97%), acetic acid (Sigma-Aldrich, 99.7%).

2.2 Instrumentation

Scanning electron microscopy (SEM) was performed on a JOEL JSM6340F scanning electron microscope. Samples for SEM were prepared by diluting solid samples with 500

μL methanol and placing 2.0 μL droplet onto silica wafer and drying under a heat lamp. Transmission electron microscopy (TEM) was performed on a JEOL JEM2010F electron microscope operated at 200kV. Samples for TEM were prepared by diluting solid samples with 500 μL methanol and placing 2.0 μL droplets onto carbon-coated copper grids and drying under a heat lamp. Nuclear magnetic resonance spectroscopy (NMR) was performed on Varian 500 MHz and 600 MHz NMR spectrometers. Samples for CTAB amount NMR measurement were prepared by soaking CTAB capped Pd NPs with 650 μL 50.00 mM 2-mim D_2O solution and taking 630 μL supernatant D_2O solution into normal glass NMR tube after centrifugation with 20 μL 30.00 mM methylsulfonyl-methane as internal standard. Samples for crotonaldehyde conversion NMR measurement were prepared by mixing 40 μL reaction solution with 610 μL $CDCl_3$ and transferring in normal glass NMR tube. All of the ^1H NMR measurements were performed with 90-degree pulse and a recycle delay larger than 5 times of spin-lattice relaxation time (5T1, ~70s) between each transient to ensure complete relaxation of the observed spins. Surface Enhanced Raman Spectroscopy (SERS) was performed on a Micro-Raman system (XploRA, Horiba) with 635 nm laser excitation. Samples for SERS acquisition were liquid phase mixture solution with Au NPs and other chemicals in light-tight container. Dynamic light scattering measurement was carried out on DynaPro NanoStar 119-DPN (Wyatt) in a quartz cuvette, calibrating with toluene and measuring solvent offset with 1% ethanol water solution.

2.3 Synthesis of Materials

Synthesis of CTAB capped Pd nanocubes

50 mg CTAB was dissolved in 9.3 ml deionized water following by adding 0.5 ml 0.01 M H_2PdCl_4 solution. The mixture solution was placed in 95 ℃ oil bath for 5 minutes and 200 μL 0.04 M ascorbic acid was added under 200 rpm stirring. The solution was heated at 95 ℃ under stirring for 30 minutes and spun down at 8000 rpm for 15 minutes. Normally, 10 batches of Pd NPs were synthesized and redispersed in 5 ml deionized water (10 mM).

Synthesis of CTAB capped Au nanooctahedron

550 mg CTAB was dissolved in 97 ml deionized water. Then, 2.5 ml 0.01 M $HAuCl_4$ solution and 0.5 ml 0.1 M trisodium citrate solution were added. The mixture solution was transferred into a 200 ml pressure vessel and heated in oven at 110 ℃ for 24 hours. The formed CTAB capped Au NPs were centrifuged down at 8000 rpm for 20 minutes and redispersed in 2.5 ml deionized water (10 mM).

Synthesis of CTAC capped Au nanocubes

CTAC capped Au nanocubes were synthesized following the seed-mediated synthesis method from the previous report with some modifications.40 For the synthesis of Au seeds, 320 mg CTAC was dissolved in 9.75 ml deionized water, following by adding 250 μL 0.01 M $HAuCl_4$ and 450 μL 0.02 M $NaBH_4$ under stirring. The Au seed solution was aged for 1 hour at room temperature. Two batches same growth solutions were prepared by dissolving 320 mg CTAC in 9.625 ml deionized water following by adding 90 μL 0.04 M L-ascorbic acid and 250 μL 0.01 M $HAuCl_4$ and 10 μL 0.01 M sodium bromide solution. 105 μL seed solution was added to the first growth solution. Shook until pink

color was present and immediately transfer 25 μL into the second growth solution. Stirred the second growth solution for 10 seconds and let it sit for 15 minutes. Normally, 20 batches of CTAC capped Au nanocubes were synthesized, centrifuged and redispersed in 5 ml deionized water which leaded to 10 mM Au NPs suspension.

Synthesis of CTAB capped Ag nanoparticles

The synthesis was carried out following the previous report with some modifications. 43 0.51 g $AgNO_3$ was dissolved in 50 ml deionized water followed by adding 1.0 M aqueous ammonia in a dropwise manner until a clear colorless solution was obtained. Then, the solution was transferred into a 100-ml volumetric flask quantitatively and was made up to 100 ml with deionized water. Finally, the $[Ag(NH_3)_2]OH$ solution was 30.00 mM. 2.5 ml freshly made $[Ag(NH_3)_2]OH$ was transfer into a 75 ml pressure vessel. 10 ml deionized water, 2.5 ml of 20 mM glucose, and 3 ml of 50 mM CTAB solutions were added under stirring. The pressure vessel was heated at 120 ℃ in a furnace for 8 hours. After cooling down to room temperature, the solution was centrifuged at 8000 rpm and redispersed into 7.5 ml deionized water to make the concentration 10 mM.

Synthesis of one-to-one NP@ZIF-8 core-shell structure

For different metal NPs, similar synthetic procedure was carried out. 1.58 M 2-mim and 0.40 mM CTAB aqueous solutions were mixed in a 1:1 manner to obtain mixture solution with 0.79 M 2-mim and 0.20 mM CTAB. 0.25 ml 10 mM metal NPs was centrifuged down at 8000 rpm for 10 minutes and redispersed into 0.5 ml deionized water. 1.75 ml 2-mim/CTAB mixture solution and 0.25 ml 97.5 mM $Zn(NO_3)_2$ solution were

mixed in a 20 ml glass vial under 500 rpm stirring at room temperature, 10 seconds after which 0.5 ml redispersed metal NPs suspension was added. After stirring for 5 minutes, let the solution sit for 3 hours. The final solution was spun down at 6000 rpm for 10 minutes and washed with methanol for three times.

Synthesis of one-to-one Au@UiO-66

200 μL 10 mM CTAC capped Au NPs was centrifuged at 8000 rpm for 10 minutes and washed with 100 μL deionized water once and was finally redispersed into 100 μL deionized water. 0.36 M 4F-BDC and $ZrOCl_2$ solutions were pre-pared by dissolving mg 4F-BDC and mg $ZrOCl_2$ in 0.5 ml 6 M acetic acid respectively. Both solutions were pre-heated in 50 ℃ oil bath for around 5 minutes followed by adding $ZrOCl_2$ solution into 4F-BDC solution under 200 rpm stirring at 50 ℃. After stirring for one minute, 100 μL washed Au NPs water solution was introduced. The stir bar was taken out after stirring for another 1 minute and the mixture solution was left in 50 ℃ oil bath for 3 hours. The resulted product was obtained by centrifugation at 4000 rpm for 10 minutes and washed with DMF once and methanol twice.

CTAB to CTAC capping agents exchange

375μL 10 mM CTAB capped Au NPs was centrifuged down at 8000 rpm for 10 minutes and redispersed in 100 μL 100 mM CTAC aqueous solution. The Au NPs suspension was left sit at room temperature overnight. It was spun down at 8000 rpm for 10 minutes and washed with 100 μL deionized water once and finally dispersed in 100 μL deionized

water, waiting for encapsulation. The control was done similarly while the only difference was 100 mM CTAB solution was used to soak Au NPs.

2.4 Characterization and Analysis

CTAB amount measurement by NMR

0.25 ml CTAB capped Pd NPs solution was taken and centrifuged at 12000 rpm for 15 minutes. After removal of supernatant, 0.5 ml 50.00 mM 2-mim solution (D_2O as solvent) was added to redisperse the Pd NPs. The Pd NPs suspension was left sit at room temperature for certain time (1, 2 or 4 hours). After that, Pd NPs suspension was centrifuged again at 12000 rpm for 15 minutes, and the supernatant was taken for ^1H NMR analysis. The quantitative measurement of absolute CTAB amount in supernatant was done by using methylsulfonylmethane (20 μL, 30.00 mM) as internal standard. All of the measurements were done with $\prod/2$ pulse and recycle delay (d_1) larger than 5 times of spin-lattice relaxation delay ($5T_1$, ~70s).

Hydrogenation of crotonaldehyde

For each catalysis, around 5 mg catalyst was weighted and redispersed into 2.1 ml isopropanol and transferred into 3.0 ml narrow-neck glass container after which 0.4 ml crotonaldehyde (≥99%) was added. The glass container was then moved into a metallic high pressure reactor followed by three times purge to remove air inside. Then the H_2 pressure was increased to 3.0 MPa. The reactor was left at room temperature for 48 hours. Catalysts were recycled by centrifugation under 6000 rpm for 10 minutes. The

supernatant solution was analyzed by 1H NMR with $CDCl_3$ as solvent, and the conversion was calculated by using ratio between reactant and products.

Chapter 3 Results and Discussion

3.1 One-to-one NP@ZIF-8 structure and synthesis

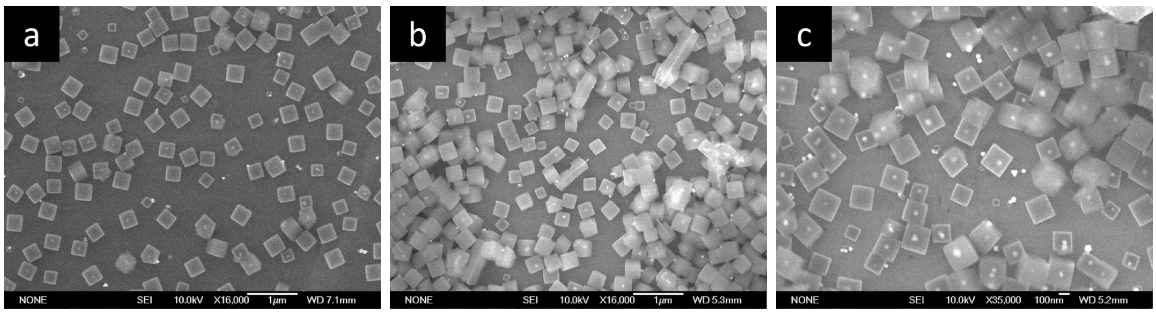

Figure 3. SEM images of (a) Au octahedron@ZIF-8. (b) Ag NPs@ZIF-8. (c) Pd sphere@ZIF-8.

Materials discussed in this article are one-to-one NP@MOF core-shell structures composed of crystalline metal NPs and zeolite imidazolate frameworks (ZIF-8). Typical one-to-one core-shell structures are shown in Figure 3 and Figure 4. The SEM image shows that metal NP is individually encapsulated in cubic single-crystalline ZIF-8 crystals (Figure 3, Figure 4g). Compared with NPs@MOF composite materials when multiple metal crystals are encased in one MOF, one-to-one NP@MOF core-shell type materials have controllable MOF coating thickness, which provides a predictable diffusion length from MOF surface to the interface formed by metal NP and MOF. This

is extremely helpful when we study reaction kinetics in which diffusion needs to be considered carefully.

On the other hand, as reported previously, in this core-shell structure, we found lattice alignment between cubic ZIF-8 crystal and metal NP with specific shapes, typically cubic Pd crystal. We concluded that {100} facet of ZIF-8 is aligned with {100} facet of Pd nanocube core, since both cubic ZIF-8 and Pd crystals are enclosed by six {100} facets, it is easy to distinguish the lattice orientation relationship between two crystalline phases.[33] Recently, for the first time according to our best knowledge, electron diffraction pattern of ZIF-8 was obtained by using our Pd@ZIF-8 sample and a set of characteristic square spot array of ZIF-8 was seen, which confirms that cubic ZIF-8 was surrounded by six well-defined {100} facets and the view direction of Figure 4b was indeed [001] as our expect (Figure 4b-c). Although, the diffraction pattern of Pd nanocube core was not obtained, previous studies have shown that Pd nanocubes synthesized under similar conditions are enclosed by {100} facets with well-defined cubic shape.[34] Thus, based on the assigned facets of cubic ZIF-8 crystal and the relative orientation of well-studied Pd nanocube inside, the alignment relationship is solid. The facet alignment between metal NPs and MOFs is rare in NP@MOF composite materials, which is fundamentally important for understanding the specific pore environment around active sites of metal NPs at the interface, and thus the catalytic properties of NPs/MOFs hybrid materials.

In a typical NP@MOF composite material synthesis procedure, quaternary ammonium surfactants (CTAB or CTAC) capped metal NPs are synthesized first. Encapsulation of

metal NPs is carried out by mixing 2-methylimidazole (2-mim) solution and Zn^{2+} solutions together, which are linker and metal node of ZIF-8 respectively, followed by introducing as-synthesized and washed metal NPs after a time interval. We applied similar synthetic strategies to CTAB or CTAC capped NPs of different components (Pd, Au and Ag) and different shapes (cube, octahedron, sphere and rod), having achieved the synthesis of one-to-one core-shell composite materials of Pd cube@ZIF-8 (Figure 4a,b), Pd sphere@ZIF-8 (Figure 4e), Au octahedron@ZIF-8 (Figure 4d) and Ag NPs@ZIF-8 (Figure 4f, Figure 5).

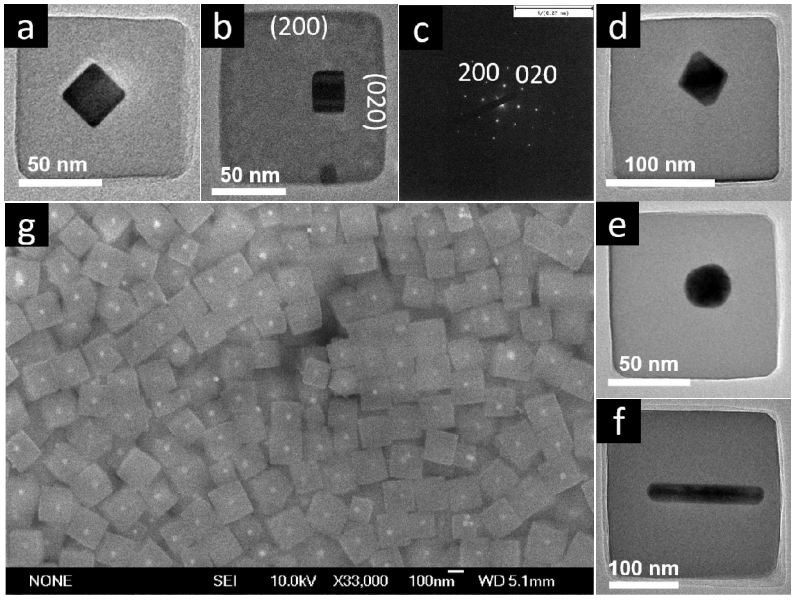

Figure 4. TEM image of (a,b) cubic Pd@ZIF-8 in [100] and [001] view direction. (c) selected area electron diffraction (SAED) of Pd@ZIF-8 shown in (b). (d) octahedral Au@ZIF-8. (e) sphere Pd@ZIF-8. (f) Ag NR@ZIF-8. (g) SEM image of cubic Pd@ZIF-8.

It is worth mentioning that Ag NPs are mixture of spheres, cubes and rods (Figure 5a), synthesized with a method based on CTAB-modified silver mirror reaction,[35] and these Ag NPs with different shapes were encased in ZIF-8 crystals in one reaction simultaneously (Figure 5). Also considering the fact that different metals (Pd, Au and Ag) can be encapsulate in ZIF-8 by same synthetic strategy, we believe that quaternary ammonium surfactants capped metal NPs (different components and shapes) are encapsulated in ZIF-8 based on the same mechanism.

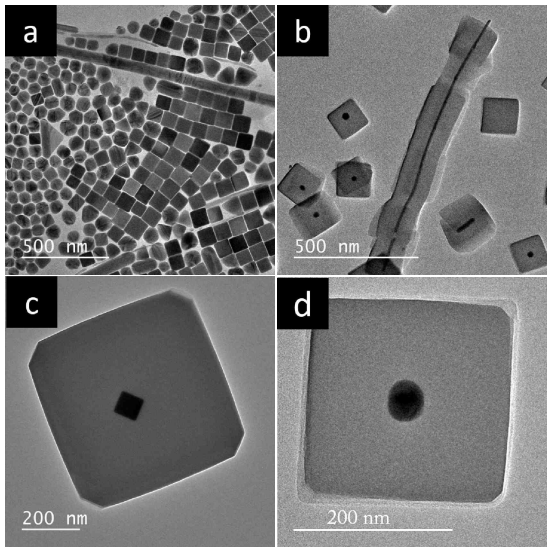

Figure 5. TEM images of (a) Ag NPs (mixture of cube, sphere and rod). (b) Ag@ZIF-8. (c) Ag cube@ZIF-8. (d) Ag sphere@ZIF-8.

Before proposing the mechanism, we obtained some indicative observation: CTAB capped Pd NPs aggregate immediately in 2-mim linker solution (Figure 6a); if Pd NPs are mixed with either 2-mim or Zn^{2+}solution first and then introduce the other, there was almost no encapsulation under SEM images and Pd NPs aggregated to the bottom (Figure 6b-e). These facts suggest that CTAB capped metal NPs are unstable under ZIF-8 water-phase synthetic condition. Thus, a mechanism based on the dissociation of CTAB from

metal NPs surface was pro-posed and many supports were found based on qualitative and quantitative analysis.

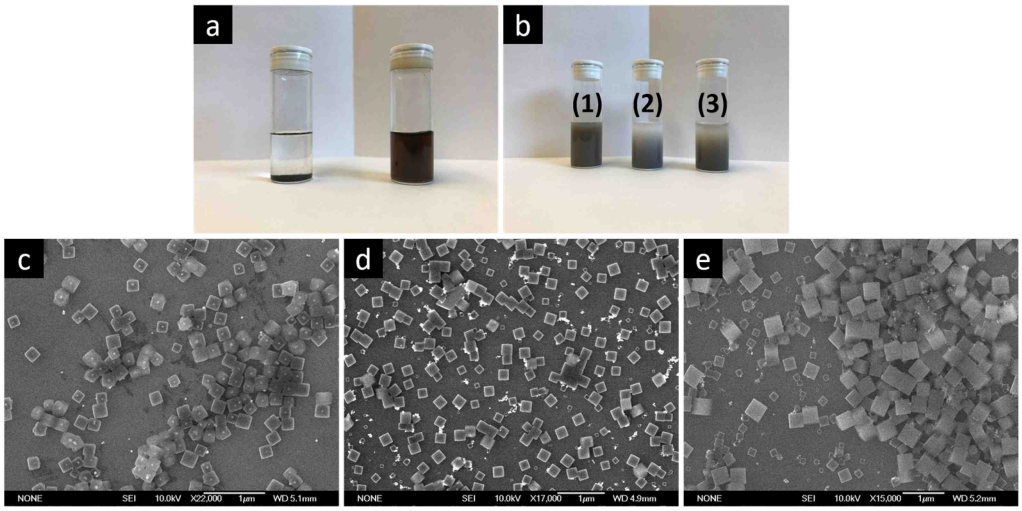

Figure 6. (a) Photograph of Pd NPs in 0.79M 2-mim solution (left) and in water (right). (b) Photograph of products by adding reagents in different sequences: (1)2-mim, Zn^{2+} and Pd NPs; (2) Zn^{2+}, Pd NPs and 2-mim; (3) 2-mim, Pd NPs and Zn^{2+}. SEM images of products resulted from different reagents adding order: (c) 2-mim, Zn^{2+} and Pd NPs. (d) Zn^{2+}, Pd NPs and 2-mim. (e) 2-mim, Pd NPs and Zn^{2+}.

3.2 Mechanism Proposed

Based on the instability of CTAB capped metal NPs mentioned above under ZIF-8 water phase synthetic condition and experiments discussed later, we proposed a mechanism of formation of one-to-one NP@ZIF-8 hybrid materials (Scheme 1). CTAB is a quaternary ammonium cationic surfactant with a sixteen-carbon chain, which is normally considered to form a bilayer structure on metal NPs surface with bromide ions bound to the metal NPs sur-face as bridges.[36] In the mechanism, CTAB molecules dissociate from metal NPs

surface as introduced into mixture solution of 2-mim and Zn^{2+}, which would lead to agglomeration if there were no alternative protective entities attach to metal NPs surface, as we observed when Pd NPs directly mixed with 2-mim solution (Figure 6a). However, under our synthetic condition, 2-mim and Zn^{2+} are mixed together before introduction of metal NPs, which leads to the generation of small ZIF-8 seeds in advance. As CTAB molecules dissociate from metal NPs surface, ZIF-8 seeds attach to the surface as another protective layer preventing metal NPs from agglomeration. After that, small ZIF-8 seeds on the surface keep taking precursors from feed solution and they reorganize together when contact with each other to form a single-crystalline ZIF-8 coating layer.

Scheme 1. Proposed mechanism for one-to-one NP@ZIF-8 formation (only one face of metal NP isshown for clearance).

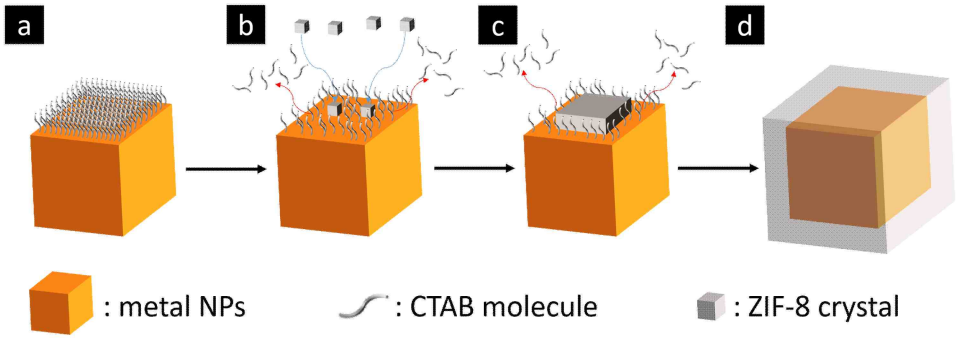

(a) Metal NP stabilized with CTAB before encapsulation. (b) Dissociation of CTAB from metal NP surface and attachment of ZIF-8 seeds onto metal NP. (c) Continuous dissociation of CTAB along with growth and reorganization of crystalline ZIF-8 shell on NPs surface. (d) Formation of one-to-one NP@ZIF-8 core-shell structure.

Supports to the mechanism have been found step by step by nuclear magnetic resonance (NMR) quantitative study of CTAB amount, surface enhanced Raman spectroscopy (SERS) study of metal NPs surface and designed control experiments.

3.3 Dissociation of CTAB Molecules

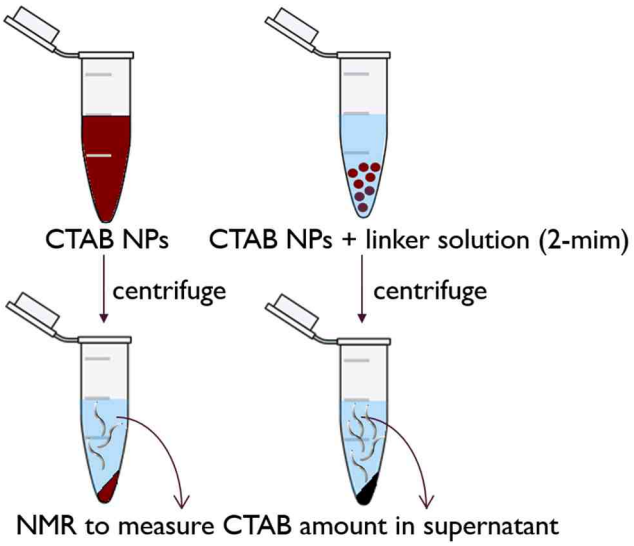

Figure 7. Descriptive graph of NMR measurement of CTAB amount in supernatants: 50.00 mM 2-mim D_2O solution was used to disperse CTAB capped Pd NPs after centrifugation. After soaking Pd NPs in 2-mim solution for a certain time interval, Pd NPs were centrifuged down to the bottom of centrifuge tube and D_2O supernatant solution was taken for ^1H NMR quantitative analysis.

Apart from observation of agglomeration of metal NPs in 2-mim solution, we used NMR to quantitatively measure the change of CTAB amount in supernatant resulting from

dissociation of CTAB molecules from metal NPs surface and the experimental procedure is shown in Figure 7. To slow down the dissociation process, CTAB capped Pd NPs were redispersed in 2-mim D_2O solution with much lower concentration, 50 mM, compared to synthetic concentration (790 mM). After a certain soaking time, Pd NPs were centrifuged down and supernatant was taken for NMR measurement. Methylsulfonylmethane (20µL, 30.00mM) was used as internal standard for quantitative NMR measurement to obtain absolute CTAB amount in the supernatant after centrifugation. As soaking time increased, the CTAB amount in the supernatant increased gradually from 0.118 µmol without soaking to 0.223 µmol after four-hour soaking. This indicates CTAB molecules continuously dissociate from Pd NPs surface in 2-mim solution (Figure 12a, black line).

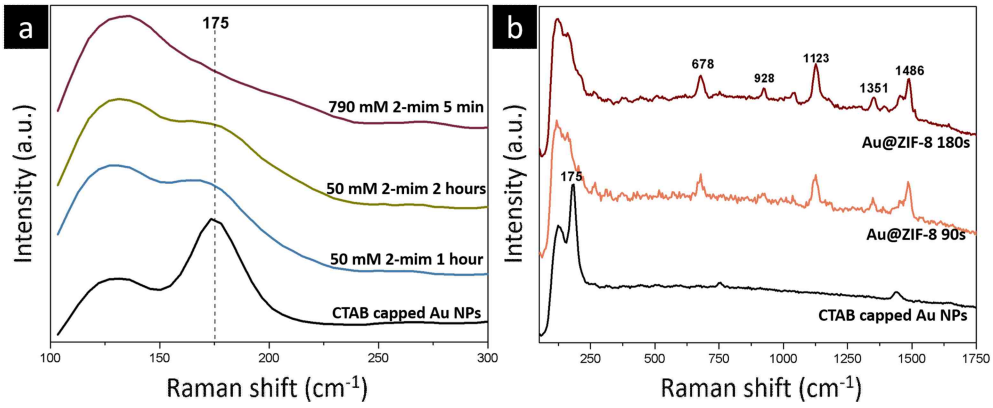

Figure 8. SERS spectrum of (a) 2-mim solution treatment of CTAB capped Au NPs: CTAB capped Au NPs (black); Au NPs soaked in 50 mM 2-mim for 1 hour (blue); Au NPs soaked in 50 mM 2-mim for 2 hours (green); Au NPs soaked in 790 mM 2-mim for 5 minutes (purple). (b) Time stage study of Au@ZIF-8 formation: CTAB capped Au NPs con-trol (black); Au@ZIF-8 90s (orange); Au@ZIF-8 180s (red).

SERS spectrum was collected by using CTAB capped Au NPs when similar 2-mim soaking conditions were applied. There was an obvious drop at 175 cm^{-1} when Au NPs was soaked in 50 mM 2-mim solution for 1 hour, which was assigned to Au-Br stretching mode because of CTAB link-age.[37-39] When 2-mim solution of synthetic condition concentration was applied (790 mM), peak at 175 cm^{-1} disappeared in 5 minutes (Figure 8a). These indicate dissociation of Br^- ion from Au NPs surface, the bridge atom between quaternary nitrogen and gold, which leads to destruction of the bilayer protective layer. In-situ SERS measurements were done under synthetic condition, peak at 175 cm^{-1} disappeared in 90 seconds after mixing Au NPs with mixture solution, while a set of peaks of 2-mim appeared (Figure 8b). The assignment of stretching mode of 2-mim is shown in Table 1. These peaks, for example 678 cm^{-1} (ν(CCH3) and 928 cm^{-1} (γ(NH)) of 2-mim, indicate the adsorption of 2-mim free molecules or surface 2-mim on ZIF-8 seeds onto Au NPs surface.[40] However, Au-N stretching mode around 225cm^{-1} was not observed, indicating that nitrogen atoms of 2-mim didn't form strong bonds with Au atoms on the surface. Also, pH value of synthetic condition is 9-11, under which 2-mim is electro-neutral (pKa1=7.86; pKa2≈15.1).[41] Based on these facts, we believe that 2-mim molecules attach on metal NPs surface via attachment of ZIF-8 seeds, which finally stabilize exposed metal NPs surface via van der Waals force.

Raman Shift (cm^{-1})	Vibrational Assignment
678	$\nu(CCH_3)$
928	γ(NH)
1123	δ(CH)
1351	ν(Ring)
1486	$\delta_{asym}(CCH_3)$

Table 1. Raman spectrum vibrational modes assignment of 2-mim from reference.[42]

The NMR and SERS results show that under synthetic condition, CTAB protective bilayer deconstructs quickly when ZIF-8 seeds attaches on metal NPs surface.

3.4 The Role CTAB Plays for Metal NP/ZIF-8 Attachment

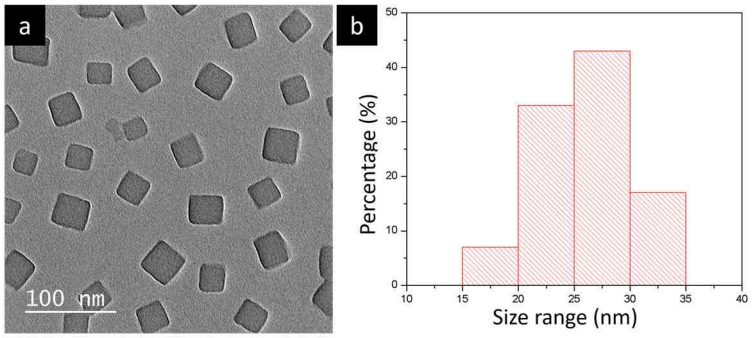

Figure 9. (a) TEM image of as-synthesized ZIF-8 particles. (b) Size distribution of as-synthesized ZIF-8 particles.

We wondered whether CTAB helped the attachment between ZIF-8 and metal NPs or not, for example as a bridge. Thus, we used as-synthesized small ZIF-8 particles (25.6 nm) (Figure 9) to mimic ZIF-8 seeds formed during the synthetic condition. As-synthesized small ZIF-8 particles were washed with methanol to remove surface CTAB and redispersed in 2-mim solution with different CTAB concentration (no CTAB, 0.2 mM, 0.4 mM, 0.6mM, 0.8mM), after which CTAB capped metal NPs were introduced (Figure 3, inset). After well mixing, hydrodynamic radius (R_H) of particles was measured by dynamic light scattering (DLS) technique (Figure 10). If there was no ZIF-8 in the mixture solution, agglomeration was observed as mentioned previously as CTAB molecules dissociate un-der high concentration 2-mim condition. But when small ZIF-8 particles existed in mixture solution, CTAB capped Pd NPs maintain the brown color in

vail 1, indicating small ZIF-8 crystals stabilized metal NPs with high sur-face energy when CTAB dissociated. As extra CTAB (0.2 mM) was mixed with 2-mim before adding metal NPs, the agglomeration of Pd NPs turned more severe as the color of suspension turned from brown to black (vial 2) and the hydrodynamic radius increased from 71.4 nm to 108.7 nm. Similar observation was obtained when concentration of CTAB increased to 0.4 and 0.6 mM (vial 3 and 4), which resulted in hydrodynamic radius value 101.4 and 104.9 nm, respectively. These results demonstrate that: firstly, when CTAB concentration is below 0.6mM, surface CTAB molecules on metal NPs still dissociate from surface; secondly, the existence of free CTAB molecules suppress the attachment of ZIF-8 particles to exposed metal NPs surface, possibly by adsorbing on ZIF-8 particle surface stabilizing {100} facet of ZIF-8 as reported in literature,[43] which leads to aggregation of Pd NPs, increasing the overall R_H.

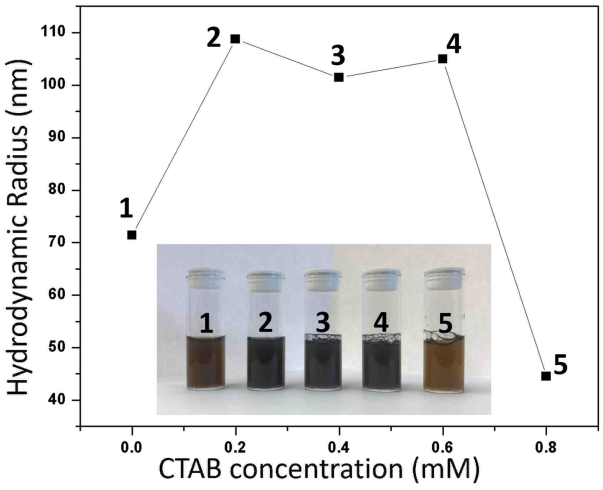

Figure 10. DLS hydrodynamic radius of particles in mixture solutions of 2-mim, small ZIF-8 and Pd NPs with increased CTAB concentration: 1) no CTAB, 2) 0.2mM CTAB, 3)

0.4mM, 4) 0.6mM and 5) 0.8mM. Inset is the photograph of mixture solutions from 1 to 5.

However, when the concentration reached to 0.8 mM, Pd NPs were well-dispersed again showing bright brown color (vial 5) with smallest R_H, 44.5 nm. This shows that dissociation of CTAB is a dynamic process and it can be suppressed when CTAB concentration in the outer environment is high.

Based on the results above, we conclude that CTAB does not help the attachment of ZIF-8 and metal NPs. It plays a role as only stabilizer of metal NPs before introducing to mixture solution in synthetic condition. And it dissociates quickly from the metal NPs surface when CTAB concentration in the solution is low (0-0.6mM), which means that extra CTAB in the solution would suppress the dissociation process.

3.5 Surface CTAB amount and poly-crystalline coating

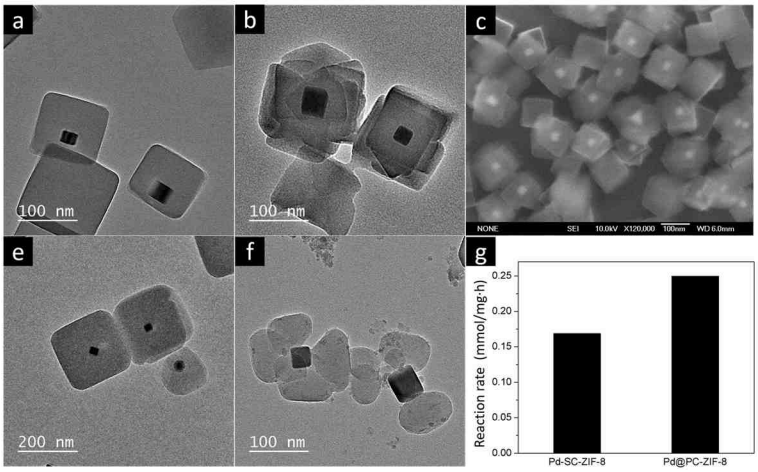

Figure 11. TEM images of (a) Pd@SC-ZIF-8. (b) Pd@PC-ZIF-8. (e) Pd@SC-ZIF-8 after catalysis. (f) Pd@PC-ZIF-8 after catalysis. (c) SEM image of Pd@PC-ZIF-8. (g) Comparison of reaction rate of crotonaldehyde hydrogenation between Pd@SC-ZIF-8 and Pd@PC-ZIF-8 (reaction rate was normalized by Pd loading amont (wt%) determined by ICP-OES).

As discussed above, introducing extra CTAB into the solution slows down the dissociation process of CTAB molecules on the metal NPs surface. We deliberately added more CTAB (20μL, 55 mM) into synthetic solution 10s after introducing metal NPs to suppress the continuous dissociation of CTAB from metal NPs surface. By doing so, Pd@poly-crystalline ZIF-8 (Pd@PC-ZIF-8) was obtained (Figure 11b and 11c). To compare catalytic performance of Pd@single-crystalline ZIF-8 (Pd@SC-ZIF-8) and Pd@poly-crystalline ZIF-8 (Pd@PC-ZIF-8), hydrogenation of crotonaldehyde was carried out with these two catalysts un-der H2 atmosphere at room temperature. The components in resulted reaction solution was analyzed by 1H NMR and the Pd loading

amount was determined by inductively coupled plasma atomic emission spectroscopy (ICP-OES). After normalizing with Pd loading amount, the reaction rates were calculated and it was found that the rate of Pd@PC-ZIF-8 was about 50% higher than Pd@SC-ZIF-8 (Table 2). The reaction rates difference can be explained by different stabilities of ZIF-8 coating shell. After the catalysis, the poly-crystalline shell broke apart and more Pd NPs surface directly exposed to outer environment (Figure 11f) compared with Pd@PC-ZIF-8 before the catalytic reaction (Figure 11b). However, single crystalline coating was still intact after catalysis (Figure 11e). It has never been reported previously that the crystallinity of MOF coating shell has an impact to the stability of NP@MOF core-shell structure, which is important for the design of stable heterogeneous catalysts. Thus, studies have been done to this Pd@PC-ZIF-8 material, trying to find the origin of the poly-crystallinity.

	Pd@SC-ZIF-8	Pd@PC-ZIF-8
Pd loading (wt %)	2.16	2.63
Amount of catalysts used for hydrogenation (mg)	5.09	4.86
Conversion of crotonaldehyde (%)	37.1	63.9
Reaction rate after normalization (mmol/mg·h)	8.12	12.0

Table 2. Reaction rate of crotonaldehyde hydrogenation comparison between Pd@SC-ZIF-8 and Pd@PC-ZIF-8. Pd loading (wt%) was determined by separated ICP-OES experiment.

SERS spectrum was collected 1min after synthetic condition of Au@PC-ZIF-8 and Au@SC-ZIF-8, respectively. The result shows that there was a shoulder peak at 175 cm^{-1}

for Au@PC-ZIF-8 while there was no signal for Au@SC-ZIF-8 (Figure 12a). This indicates that when extra CTAB molecules were introduced into the system, only not the CTAB amount in the solution increased, but also the CTAB amount on Au NPs surface. So, the next question is that which one resulted in poly-crystalline coating.

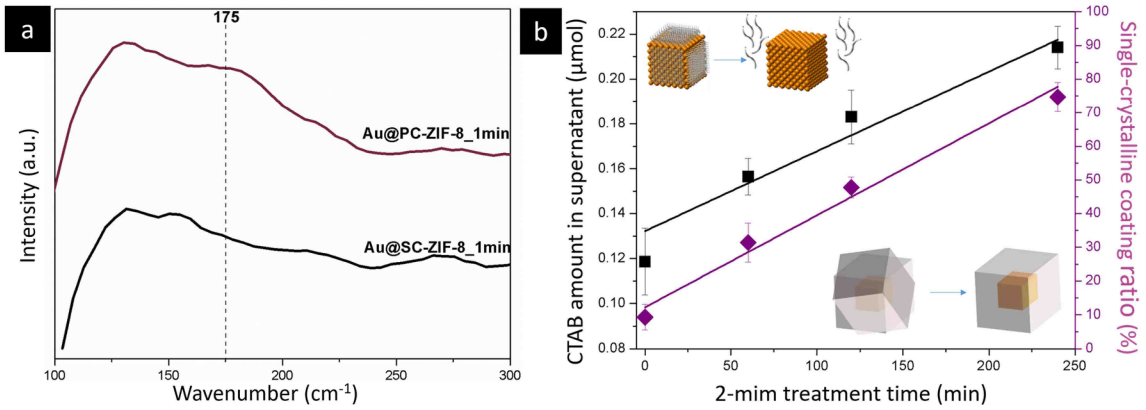

Figure 12. (a) SERS spectrum collected under synthetic condition of Au@PC-ZIF-8 and Au@SC-ZIF-8 at 1min. (b) Time-dependent CTAB amount in supernatant of 2-mim treated Pd NPs suspension measured by NMR (black) and corresponding ratio of Pd@SC-ZIF-8 in resulted products (purple).

	Trail 1			Trail 2			Trail 3			Mean of SC ratio (3 trails)
	# of SC	# of all	SC ratio	# of SC	# of all	SC ratio	# of SC	# of all	SC ratio	
No 2-mim treatment	14	103	13.6%	9	142	6.34%	9	111	8.11%	9.30%±3.75%
1 hour	24	93	25.8%	41	132	31.1%	49	131	37.4%	31.4%±5.8%
2 hours	53	108	49.1%	42	95	44.21%	64	128	50.0%	47.8%±3.1%
4 hours	42	54	77.8%	48	68	70.6%	43	56	76.8%	74.6%±4.3%

Table 3. Calculation of Pd@SC-ZIF-8 ratio in poly-crystalline coating experiment when 2-mim pretreated Pd NPs were used (treatment time was 1, 2 and 4 hours respectively).

Results shown in the table were from counting specific Pd@ZIF-8 numbers in TEM images.

To answer the question above, a control experiment was designed. Low concentration 2-mim solution (50mM) was used to pre-clean Pd NPs surface as explained above that longer the time Pd NPs was soaked in 2-mim solution, more CTAB dissociated from Pd NPs surface increasing concentration of free CTAB molecules in the solution (Figure 12b, black line). In other words, this pretreatment maintained the total CTAB amount in the system but changed the distribution of CTAB molecules, decreasing the surface CTAB amount, but increasing solution CTAB amount. And these 2-mim solution soaked Pd NPs (1 hour, 2 hours and 4 hours) were used to do the same poly-crystalline ZIF-8 coating. After the encapsulation reaction, the ratio of Pd@SC-ZIF-8 to entire Pd@ZIF-8 composite materials (both Pd@SC-ZIF-8 and Pd@PC-ZIF-8) was calculated by counting more than 100 core-shell composite materials according to TEM images (Table 3). The result is shown as purple line in Figure 5b. There is an obvious increase of single-crystalline coating ratio from 9.3% when there was no 2-mim pretreatment to 74.6% when the soaking time increased to 4 hours. This result demonstrates that less the surface CTAB amount was, less poly-crystalline coating was obtained. That is to say, when extra CTAB molecules were introduced to the solution during the poly-crystalline coating process, it was the increase of surface CTAB amount that led to poly-crystalline coating. It has never been reported that cap-ping agents amount on metal NPs surface affects the crystallinity of MOFs coating shell in NPs@MOFs core-shell hybrid materials. Our explanation to this is that CTAB molecules on metal NPs surface impede the contact of

small ZIF-8 seeds with each other which is essential for the reorganization process. Under this scenario, ZIF-8 seeds on Pd NPs surface preferentially take ZIF-8 clusters or starting materials from solution and grain boundaries form when large ZIF-8 crystals with well-defined crystal-line facets meet on Pd NPs surface and thus form poly-crystalline ZIF-8 coating. And it can be easily explained that when Pd NPs with less CTAB on the surface after 2-mim treatment were used, more Pd@SC-ZIF-8 was obtained.

3.6 Mechanism Summary

Based on discussions above, the one-to-one encapsulation of quaternary ammonium capping agent capped NP into MOF involves a dynamic dissociation process of surface capping agents. The protective layer provided by capping agent deconstructs when metal NPs are introduced into MOFs synthetic condition, where MOFs seeds in the solution attach on metal NPs as alternative isolative layer preventing metal NPs from agglomeration.

As discussed, dissociation of capping agents from metal NPs surface is critical for one-to-one encapsulation in our case. This is quite different with metal NPs@MOFs hybrid materials synthesized via "ship-around-bottle" method commonly using metal NPs with strong capping agents, like PVP, in which PVP polymer chains well protects metal NPs and facilitate the interaction between metal NPs and MOFs seeds in the solution through weak coordination interactions and hydrophobic interactions.[13]

Apart from that, the presence of small MOFs seeds in the solution is also important. For example, if the time interval we waited to add Pd NPs became longer from 10 seconds to

4 minute, ZIF-8 seeds grow by themselves in the solution before introduction of metal NPs, which resulted from less encapsulation and larger empty ZIF-8 particles (Figure 13). This could be explained by the amount of small ZIF-8 seeds which are available for exposed metal NPs became less when the time interval increased, based on kinetic studies of ZIF-8 growth.[44]

Thus, instead of protecting metal NPs well with strong capping agents, metal NPs with soft capping agent, like CTAB, can also be used under harsh MOFs synthetic condition to realize NP@MOF core-shell structure as long as small MOF seeds are present in the solution to provide alternative protection to exposed metal NPs surface with high surface energy.

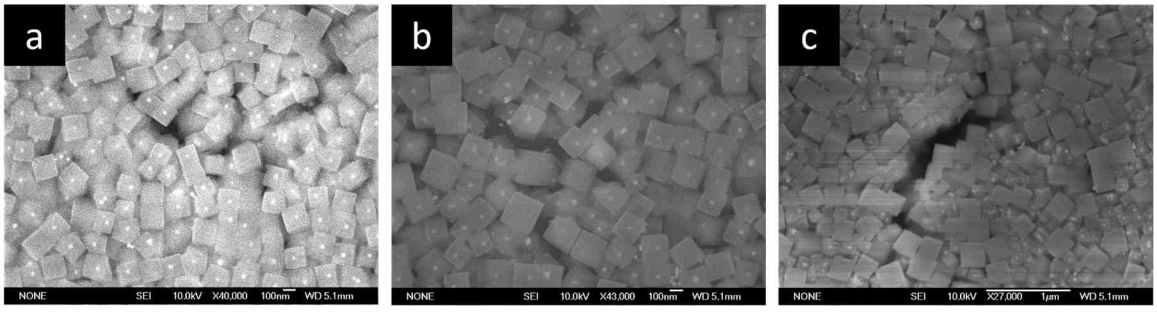

Figure 13. SEM images of Pd@ZIF-8 when Pd NPs introduced in to ZIF-8 growth solution after time interval: (a) 10s, (b) 60s, and (c) 240s.

3.7 Expand the interface understanding: Au@UiO-66

When design NP@MOF core-shell heterogeneous catalysts, a chemically and thermally robust MOF outer layer is often desired for harsh catalytic conditions, like environment with strong acidity and high temperature. Compared with ZIF-8, which would be

decomposed when the pH in the environment is below 5,[45] UiO-66 is another MOF with better chemical and thermal stability and the only effective way to entirely decompose UiO-66 is hydro-fluoric acid so far. Thus, we tried to obtain one-to-one metal NP@UiO-66 hybrid material guided by our under-standing to NP@ZIF-8 system by using similar synthetic strategy.

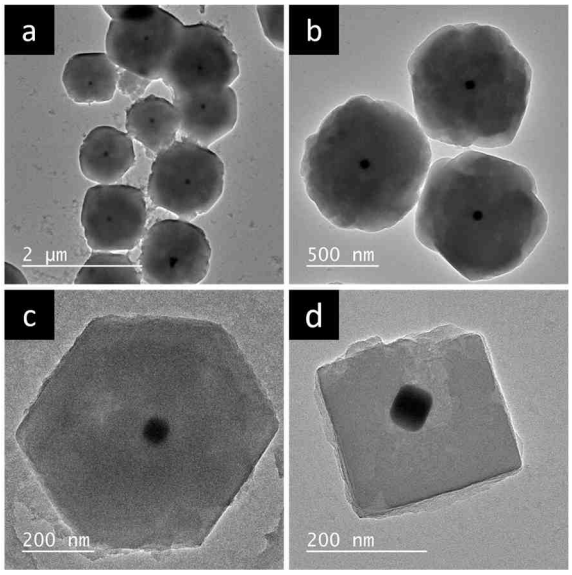

Figure 14. TEM images of CTAC capped Au@UiO-66: (a), (b) Au@UiO-66 with irregular shape. (c) Au@UiO-66 with octahedron shape. (d) Au@UiO-66 with cubic shape.

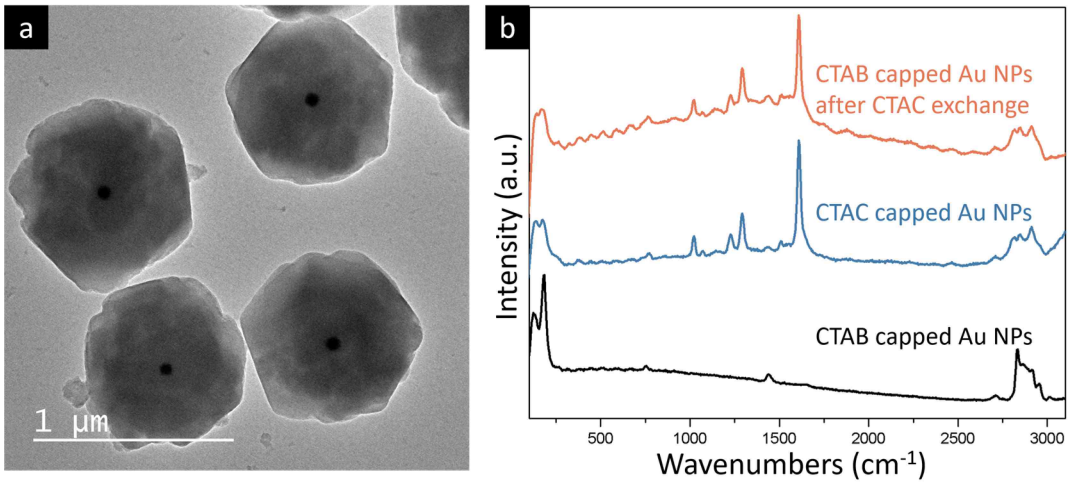

Figure 15. (a) TEM image of Au@UiO-66. (b) SERS spectrum of CTAB capped Au (black); CTAC capped Au NPs (blue) and CTAB capped Au NPs after 24 hour CTAC exchange (orange).

Based on the aqueous phase synthesis recipe of UiO-66 found by our group, zirconyl chloride octahydrate ($ZrOCl_2$) and tetrafluoroterephthalic acid (4F-BDC) were used as zirconium precursor and organic linker respectively, while acetic acid was introduced as modulator. ZrOCl2 and 4F-BDC were dissolved in 6M acetic acid separately before reaction. Similar with the synthesis of one-to-one metal NP@ZIF-8, $ZrOCl_2$ and 4F-BDC were firstly mixed together in 50℃ oil bath, and then quaternary ammonium surfactants capped metal NPs were added under stir-ring after a time interval.

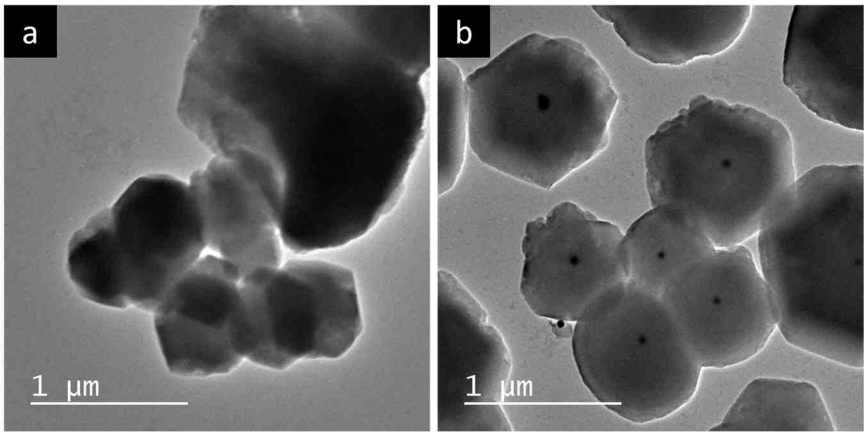

Figure 16. TEM images of Au@UiO-66 by using CTAB capped Au NPs after 100 mM (a) CTAB and (b) CTAC solution soaking treatment.

CTAB and CTAC capped Au NPs were chosen to study this proof of concept. As in Au@ZIF-8, CTAB capped Au was firstly used during the synthesis. However, Au NPs agglomerated after the reaction and UiO-66 did not encase Au NPs (Figure 16a). According to our understanding as discussed above, dissociation of CTAB is a critical step for the encapsulation. Thus, facilitating dissociation of quaternary ammonium surfactants from Au NPs sur-face is one possible method to promote the encapsulation. According to previous experimental studies, the binding strength of Au-Cl^- is weaker than Au-Br^-.[46-48] So, CTAC capped Au NPs was synthesized by seed-mediated method reported previously,[49] and it was found that encapsulation of Au NPs into UiO-66 was successful when CTAC was used as the capping agents (Figure 14, Figure 15a). And also, capping agents exchange was carried out to replace original CTAB molecules on the Au surface with CTAC molecules: as-synthesized CTAB capped Au NPs were centrifuged down and dispersed in CTAC solution for 24 hours, while in CTAB solution as the control. Only the one treated with CTAC solution was successfully encapsulated in

UiO-66 under the same synthetic condition while no encapsulation was observed for CTAB soaked Au NPs (Figure 16).

To confirm the successful capping agents exchange, SERS spectrums were collected for as-synthesized CTAB capped Au NPs, CTAC capped Au NPs and CTAB capped Au NPs after CTAC exchange (Figure 15b). For CTAC capped Au NPs, the Au-Br stretching peak at 175 cm^{-1} was very weak, which was possibly resulted from trace amount of bromide ion impurity in CTAC powder chemicals (95% purity). And similar weak peak at the same position was present in CTAC exchanged Au NPs as well, indicating dissociation of the majority of Br^- ions from Au NPs surface after the surfactants exchange. However, Au-Cl stretching mode around 265 cm^{-1} was not observed and has never been reported for CTAC on Au NPs, which might because of the weak bonding between the chlorine ion at quaternary ammonium end of CTAC and Au atom on NPs surface.[50] Peaks at 1023, 1220 and 1295 cm^{-1} were assigned as C-C stretching, CH_2 wag and CH_2 twist modes of CTA^+, respectively.[51] These peaks were present in CTAC capped Au NPs and CTAC exchanged Au NPs, but not in CTAB capped Au NPs. This indicates that: firstly, arrangement of CTAB and CTAC on Au NPs might be different because of different binding affinities of halide ions which leads to the fact that only stretching modes at quaternary ammonium end got enhanced for CTAB while certain stretching modes on carbon chain were enhanced for CTAC; secondly, CTAB molecules on as-synthesized CTAB capped Au NPs surface were indeed replaced by CTAC molecules. This supports our understanding that the configuration and behavior of capping agents on metal NPs surface indeed affects the formation of MOF coating shell.

Chapter 4. Conclusion and Outlook

A novel synthetic strategy of NP@MOF core-shell structure was proposed based on mechanism study of metal NP@ZIF-8 one-to-one core-shell hybrid materials. Compared with previous NP@MOF synthetic conditions, where strong capping agents well protect metal NPs un-der MOFs synthetic conditions, dissociation of capping agents from metal NPs surface and direct attachment of MOF particles and metal NPs are important for successful encapsulation in our synthetic strategy. As what we observed, when the dissociation of capping agent, CTAB molecules, were interrupted during the synthesis, the crystallinity and stability of MOFs coating shell was affected. Thus, we believe that to form a NP@MOF core-shell structure with fine interface environment, dissociation of capping agents and direct contact between metal NPs and MOFs are essential. And a direct contact interface between MOFs and metal NPs is vital for studies which want to control catalytic properties of NPs@MOFs core-shell hybrid materials by changing pore environment of MOFs through their tunability. In the end, it is promising that this synthetic strategy and our understanding has potential to be compatible to other MOFs system, like UiO-66 discussed above, which is very helpful for the design of novel NP@MOF core-shell composite materials.

Reference

(1) Hoener, C. F.; Allan, K. A.; Bard, A. J.; Campion, A.; Fox, M. A.; Mallouk, T. E.; Webber, S. E.; White, J. M. *The Journal of Physical Chemistry* **1992**, *96*, 3812.

(2) Spanhel, L.; Weller, H.; Henglein, A. *Journal of the American Chemical Society* **1987**, *109*, 6632.

(3) Dabbousi, B. O.; Rodriguez-Viejo, J.; Mikulec, F. V.; Heine, J. R.; Mattoussi, H.; Ober, R.; Jensen, K. F.; Bawendi, M. G. *The Journal of Physical Chemistry B* **1997**, *101*, 9463.

(4) Hendon, C. H.; Rieth, A. J.; Korzyński, M. D.; Dincă, M. *ACS Central Science* **2017**.

(5) Hu, P.; Morabito, J. V.; Tsung, C.-K. *Acs Catalysis* **2014**, *4*, 4409.

(6) Yin, L.; Liebscher, J. *Chemical Reviews* **2007**, *107*, 133.

(7) Köhler, K.; Heidenreich, R. G.; Krauter, J. G.; Pietsch, J. *Chemistry-A European Journal* **2002**, *8*, 622.

(8) Liu, P.; Qin, R.; Fu, G.; Zheng, N. *Journal of the American Chemical Society* **2017**, *139*, 2122.

(9) Wu, B.; Huang, H.; Yang, J.; Zheng, N.; Fu, G. *Angewandte Chemie* **2012**, *124*, 3496.

(10) Kwak, J. H.; Hu, J.; Mei, D.; Yi, C.-W.; Kim, D. H.; Peden, C. H.; Allard, L. F.; Szanyi, J. *Science* **2009**, *325*, 1670.

(11) Kyriakou, G.; Boucher, M. B.; Jewell, A. D.; Lewis, E. A.; Lawton, T. J.; Baber, A. E.; Tierney, H. L.; Flytzani-Stephanopoulos, M.; Sykes, E. H. *Science(Washington)* **2012**, *335*, 1209.

(12) Liu, P.; Zhao, Y.; Qin, R.; Mo, S.; Chen, G.; Gu, L.; Chevrier, D. M.; Zhang, P.; Guo, Q.; Zang, D. *Science* **2016**, *352*, 797.

(13) Lu, G.; Li, S.; Guo, Z.; Farha, O. K.; Hauser, B. G.; Qi, X.; Wang, Y.; Wang, X.; Han, S.; Liu, X. *Nature chemistry* **2012**, *4*, 310.

(14) Zhang, W.; Lu, G.; Cui, C.; Liu, Y.; Li, S.; Yan, W.; Xing, C.; Chi, Y. R.; Yang, Y.; Huo, F. *Advanced Materials* **2014**, *26*, 4056.

(15) Aijaz, A.; Akita, T.; Tsumori, N.; Xu, Q. *Journal of the American Chemical Society* **2013**, *135*, 16356.

(16) Esken, D.; Turner, S.; Lebedev, O. I.; Van Tendeloo, G.; Fischer, R. A. *Chemistry of Materials* **2010**, *22*, 6393.

(17) Jiang, H.-L.; Akita, T.; Ishida, T.; Haruta, M.; Xu, Q. *Journal of the American Chemical Society* **2011**, *133*, 1304.

(18) Jiang, H.-L.; Liu, B.; Akita, T.; Haruta, M.; Sakurai, H.; Xu, Q. *Journal of the American Chemical Society* **2009**, *131*, 11302.

(19) Mukoyoshi, M.; Kobayashi, H.; Kusada, K.; Hayashi, M.; Yamada, T.; Maesato, M.; Taylor, J. M.; Kubota, Y.; Kato, K.; Takata, M. *Chemical Communications* **2015**, *51*, 12463.

(20) Sugikawa, K.; Nagata, S.; Furukawa, Y.; Kokado, K.; Sada, K. *Chemistry of Materials* **2013**, *25*, 2565.

(21) Tsuruoka, T.; Kawasaki, H.; Nawafune, H.; Akamatsu, K. *ACS applied materials & interfaces* **2011**, *3*, 3788.

(22) Kuo, C.-H.; Tang, Y.; Chou, L.-Y.; Sneed, B. T.; Brodsky, C. N.; Zhao, Z.; Tsung, C.-K. *Journal of the American Chemical Society* **2012**, *134*, 14345.

(23) Lalonde, M.; Bury, W.; Karagiaridi, O.; Brown, Z.; Hupp, J. T.; Farha, O. K. *Journal of Materials Chemistry A* **2013**, *1*, 5453.

(24) Bury, W.; Fairen-Jimenez, D.; Lalonde, M. B.; Snurr, R. Q.; Farha, O. K.; Hupp, J. T. *Chemistry of Materials* **2013**, *25*, 739.

(25) Karagiaridi, O.; Bury, W.; Mondloch, J. E.; Hupp, J. T.; Farha, O. K. *Angewandte Chemie International Edition* **2014**, *53*, 4530.

(26) Karagiaridi, O.; Bury, W.; Sarjeant, A. A.; Stern, C. L.; Farha, O. K.; Hupp, J. T. *Chemical Science* **2012**, *3*, 3256.

(27) Morabito, J. V.; Chou, L.-Y.; Li, Z.; Manna, C. M.; Petroff, C. A.; Kyada, R. J.; Palomba, J. M.; Byers, J. A.; Tsung, C.-K. *Journal of the American Chemical Society* **2014**, *136*, 12540.

(28) Takaishi, S.; DeMarco, E. J.; Pellin, M. J.; Farha, O. K.; Hupp, J. T. *Chemical Science* **2013**, *4*, 1509.

(29) Li, Z.; Schweitzer, N. M.; League, A. B.; Bernales, V.; Peters, A. W.; Wang, T. C.; Miller, J. T.; Vjunov, A.; Fulton, J. L.; Lercher, J. A. *J. Am. Chem. Soc* **2016**, *138*, 1977.

(30) Lim, B. S.; Rahtu, A.; Gordon, R. G. *Nature materials* **2003**, *2*, 749.

(31) Hwang, Y. K.; Hong, D. Y.; Chang, J. S.; Jhung, S. H.; Seo, Y. K.; Kim, J.; Vimont, A.; Daturi, M.; Serre, C.; Férey, G. *Angewandte Chemie International Edition* **2008**, *47*, 4144.

(32) McDonald, T. M.; Lee, W. R.; Mason, J. A.; Wiers, B. M.; Hong, C. S.; Long, J. R. *Journal of the American Chemical Society* **2012**, *134*, 7056.

(33) Hu, P.; Zhuang, J.; Chou, L.-Y.; Lee, H. K.; Ling, X. Y.; Chuang, Y.-C.; Tsung, C.-K. *Journal of the American Chemical Society* **2014**, *136*, 10561.

(34) Niu, W.; Zhang, L.; Xu, G. *Acs Nano* **2010**, *4*, 1987.

(35) Yu, D.; Yam, V. W.-W. *Journal of the American Chemical Society* **2004**, *126*, 13200.

(36) Nikoobakht, B.; El-Sayed, M. A. *Langmuir* **2001**, *17*, 6368.

(37) Nikoobakht, B.; El-Sayed, M. A. *The Journal of Physical Chemistry A* **2003**, *107*, 3372.

(38) Joa, S. L.; Pemberton, J. E. *The Journal of Physical Chemistry* **1993**, *97*, 9420.

(39) Boca, S. C.; Astilean, S. *Nanotechnology* **2010**, *21*, 235601.

(40) Jang, N.-H. *Bulletin of the Korean Chemical Society* **2002**, *23*, 1790.

(41) Takeuchi, Y.; Kirk, K. L.; Cohen, L. A. *The Journal of Organic Chemistry* **1978**, *43*, 3570.

(42) Carter, D. A.; Pemberton, J. E. *Journal of Raman spectroscopy* **1997**, *28*, 939.

(43) Pan, Y.; Heryadi, D.; Zhou, F.; Zhao, L.; Lestari, G.; Su, H.; Lai, Z. *CrystEngComm* **2011**, *13*, 6937.

(44) Cravillon, J.; Schröder, C. A.; Nayuk, R.; Gummel, J.; Huber, K.; Wiebcke, M. *Angewandte Chemie* **2011**, *123*, 8217.

(45) Zhuang, J.; Kuo, C.-H.; Chou, L.-Y.; Liu, D.-Y.; Weerapana, E.; Tsung, C.-K. *ACS nano* **2014**, *8*, 2812.

(46) Niidome, Y.; Nakamura, Y.; Honda, K.; Akiyama, Y.; Nishioka, K.; Kawasaki, H.; Nakashima, N. *Chemical Communications* **2009**, 1754.

(47) Atkin, R.; Craig, V.; Wanless, E. J.; Biggs, S. *Journal of colloid and interface science* **2003**, *266*, 236.

(48) Patrick, H. N.; Warr, G. G.; Manne, S.; Aksay, I. A. *Langmuir* **1999**, *15*, 1685.

(49) Wu, H.-L.; Kuo, C.-H.; Huang, M. H. *Langmuir* **2010**, *26*, 12307.

(50) Corma, A.; Concepción, P.; Domínguez, I.; Forné, V.; Sabater, M. J. *Journal of Catalysis* **2007**, *251*, 39.

(51) Dendramis, A.; Schwinn, E.; Sperline, R. *Surface science* **1983**, *134*, 675.